Tailoring the Spatio-temporal Bandwidth of Biphotons via the Non-factorable Structure of Entanglement

L. Caspani, E. Brambilla, L.A. Lugiato, and A. Gatti

CNR-INFM and CNISM, Dipartimento di Fisica e Matematica,
Università dell'Insubria,
Via Valleggio 11, Como, Italy
alessandra.gatti@mi.infn.it

Abstract. We investigate the spatio-temporal structure of the biphoton entanglement in Parametric Down Conversion (PDC). In particular we study the biphoton amplitude at the output face of the nonlinear crystal (near-field) and we demonstrate its X-shaped geometry in the space-time dimensions, i.e. the non-factorability of the state with respect to spatial and temporal variables. Our analysis provides a precise and quantitative characterization of this structure in various regimes and types of phase matching of PDC. The key elements of novelty emerging from our analysis are the non-factorability of the state with respect to spatial and temporal variables, and the extreme relative localization of the entangled photons, both in space (few microns) and time (few femtoseconds). This extreme localization is connected to our ability to resolve the photon positions in the source near-field. The non factorability opens the possibility of tailoring the temporal entanglement by acting on the spatial degrees of freedom of twin photons.

Keywords: Quantum entanglement, Parametric Down-Conversion, Biphoton correlation.

1 Introduction

Parametric down-conversion (PDC) is probably the most efficient and widely used source of entangled photon pairs, which have been employed in several successful implementations of quantum communication and information schemes. At the very heart of such technologies lies the quantum interference between photonic wave functions, which depends crucially on the spatio-temporal mode structure of the photons. In dependence of the application under consideration, different properties of the entangled photons (e.g the spectral bandwidth) are enhanced. For example, recently proposed protocols for long-distance quantum communication based on photon-atom interaction require narrowband biphotons [1, 2], with linewidth less than the atomic linewidth ($\sim$ MHz [3, 4]), whereas ultra-broadband biphotons ($\sim$ GHz) are required for high-axial-resolution quantum optical coherence tomography [5, 6], or for clock synchronization protocols [7, 8].

A. Sergienko, S. Pascazio, and P. Villoresi (Eds.): QuantumCom 2009, LNICST 36, pp. 1–16, 2010.

Different methods were proposed in last years to generate broadband biphotons, and more in general to taylor their spectral properties. Some of them exploits the properties of the nonlinear medium, by choosing a very thin crystal [9], or using chirped quasi-phase-matched nonlinear gratings [10, 11, 12, 13]. In other works the spectral properties of biphotons were controlled thanks to pump engineering, by choosing appropriately the pump wavelength [14, 15], acting on its spatial properties and exploiting the non-collinear phase matching configuration [16, 17, 18] or, more recently, by mean of a tilted pump pulse [19].

In this work, the issue of controlling and tailoring the biphoton spatio-temporal structure is addressed from a peculiar and novel point of view, that is, the non factorability in space and time of the PDC biphoton entanglement. The idea comes from the context of nonlinear optics, where recent studies [20, 21] outlined how in nonlinear media the angular dispersion relations impose a hyperbolic geometry involving both temporal and spatial degrees of freedom in a non-factorable way. The wave object that captures such a geometry is the so-called X-wave (the X being formed by the asymptotes of the hyperbola), which is a localized and propagation-invariant wave-packet, non separable in space and time. The statistical counterpart of the X-wave was recently shown [22, 23] to emerge in the X-shaped structure of the coherence function, describing the classical phase coherence of the individual signal (idler) field.

In this paper, we turn our attention to the genuine quantum level, investigating the spatio-temporal structure of the biphoton cross-correlation, the quantity that is at the heart of the photon-pair PDC entanglement. We shall demonstrate that a X-geometry emerges in this microscopic context as well. With few exceptions [24, 25], the PDC entanglement has been to date investigated mostly either in a purely temporal [26, 27, 28] or spatial [29, 30, 31, 32] framework. Our approach, based on the non-factorability in space and time of the state, will point out a key element of novelty, i.e. the possibility of tailoring the temporal bandwith of the biphotons by manipulating their spatial degrees of freedom. In particular, by resolving their near-field positions, we will show that the X-structure opens the access to an ultra-broad bandwidth entangled photonic source, with a temporal localization in the femtosecond range. Our results compare with recent findings [12], where a $\sim$ 7fs Hong-Ou-Mandel dip was observed through the use of a quasi-phase-matched nonlinear grating.

2 Type I Parametric Down Conversion

We first focus on type I parametric down conversion, i.e. we consider the signal and idler fields having ordinary polarization. We consider basically the same model adopted by Gatti *et al.*[25, 32, 31]. A coherent and quasi-monochromatic pump field propagates along the z axis in a $\chi^{(2)}$ nonlinear crystal of lentgh l_c. We denote by $\hat{A}_p(\vec{x},t,z)$ and $\hat{A}_s(\vec{x},t,z)$ the envelope operator for the pump and signal field, of central frequencies ω_p and $\omega_s = \omega_p/2$, respectively:

$$\hat{A}_j(\vec{x},t,z) = \hat{E}_j^{(+)}(\vec{x},t,z)\mathrm{e}^{i\omega_j t} \quad (j=s,p)\,, \tag{1}$$

where $\hat{E}_j^{(+)}$ is the positive frequency part of the field operator, and $\vec{x} = (x, y)$ represents the transverse coordinates, while t is the time. We next pass to the Fourier domain:

$$\hat{A}_j(\vec{q}, \Omega, z) = \int \frac{d^2\vec{x}}{2\pi} \int \frac{dt}{\sqrt{2\pi}} \, \mathrm{e}^{-i\vec{q}\cdot\vec{x}+i\Omega t} \hat{A}_j(\vec{x}, t, z) \,, \tag{2}$$

where $\vec{q}$ represents the transverse component of the wave vector and Ω is the frequency offset from the carriers ω_j. In addition we extract the fast variation along z due to the linear propagation inside the crystal:

$$\hat{A}_j(\vec{q}, \Omega, z) = \mathrm{e}^{ik_{jz}(\vec{q},\Omega)z} \hat{a}_j(\vec{q}, \Omega, z) \,, \tag{3}$$

where $k_{jz}(\vec{q}, \Omega) = \sqrt{k_j^2(\vec{q}, \omega_j + \Omega) - q^2}$ is the projection of the wave vector of the j-th field along the z axis and $k_j(\vec{q}, \omega_j + \Omega)$ is the corresponding wave number. The fields $\hat{a}_j$ defined in Eq. (3) have thus a slow variation along the crystal, due only to the nonlinear interaction. In the following we assume that the pump beam is undepleted by the nonlinear interaction, i.e. $\hat{a}_p(\vec{q}, \Omega, z) = \hat{a}_p(\vec{q}, \Omega, 0)$. Moreover, since we consider as pump an intense coherent beam, the field operator can be replaced by its classical mean value: $\hat{a}_p(\vec{q}, \Omega, 0) \to \alpha_p(\vec{q}, \Omega)$. In this way the pump evolution along the crystal is simply detrmined by the linear propagation, $\mathcal{A}_p(\vec{q}, \Omega, z) = \mathrm{e}^{ik_{pz}(\vec{q},\Omega)z} \alpha_p(\vec{q}, \Omega)$.

The evolution of the signal field $\hat{a}_s$ due to the non linear interaction is described by the following equation [25]:

$$\frac{\partial \hat{a}_s(\vec{q}, \Omega, z)}{\partial z} = \frac{g}{l_c} \int \frac{d^2\vec{q}'}{2\pi} \int \frac{d\Omega'}{\sqrt{2\pi}} \bar{\alpha}_p(\vec{q} + \vec{q}', \Omega + \Omega') \hat{a}_s^\dagger(\vec{q}', \Omega', z) \mathrm{e}^{-i\Delta(\vec{q},\Omega;\vec{q}',\Omega')z} \,, \tag{4}$$

where $\bar{\alpha}_p$ represents the pump field (at the input face of the crystal) normalized to its peak value α_p, and $g = \chi^{(2)} \alpha_p l_c$ is the dimensionless parametric gain, with $\chi^{(2)}$ being a parameter proportional to the second-order susceptibility of the medium. The phase mismatch function, defined as

$$\Delta(\vec{q}, \Omega; \vec{q}', \Omega') = k_{sz}(\vec{q}, \Omega) + k_{sz}(\vec{q}', \Omega') - k_{pz}(\vec{q} + \vec{q}', \Omega + \Omega') \,, \tag{5}$$

determines the efficiency of the down-conversion process, in which a pump photon of frequency $\omega_p + \Omega + \Omega'$ with transverse wave vector $\vec{q} + \vec{q}'$, splits into two signal photons of frequencies $\omega_s + \Omega$ and $\omega_s + \Omega'$, with wave vectors $\vec{q}$ and $\vec{q}'$, respectively.

We can find an analytic solution of Eq. (4), if we consider a plane and monochromatic pump, i.e. $\bar{\alpha}_p(\vec{q}, \Omega) = (2\pi)^{3/2} \delta(\vec{q}) \delta(\Omega)$ (an analysis for a nearly monochromatic pump that leads to similar results can be found in [33, 34]). In this case, indeed, the solution can be expressed by mean of the usual input-output relations [25]:

$$\hat{A}_s(\vec{q}, \Omega) = U(\vec{q}, \Omega) \hat{A}_s(\vec{q}, \Omega, 0) + V(\vec{q}, \Omega) \hat{A}_s^\dagger(-\vec{q}, -\Omega, 0) \,, \tag{6}$$

where, if not differently stated, the fields are evaluated at $z = l_c$ (near-field), and

$$U(\vec{q},\Omega) = \mathrm{e}^{i\frac{k_p l_c}{2}}\mathrm{e}^{i\varphi(\vec{q},\Omega)}\left\{\cosh\left[\Gamma(\vec{q},\Omega)\right] + i\frac{\Delta_{\mathrm{pw}}(\vec{q},\Omega)l_c}{2\Gamma(\vec{q},\Omega)}\sinh\left[\Gamma(\vec{q},\Omega)\right]\right\}, \tag{7a}$$

$$V(\vec{q},\Omega) = \mathrm{e}^{i\frac{k_p l_c}{2}}\mathrm{e}^{i\varphi(\vec{q},\Omega)}\frac{g}{\Gamma(\vec{q},\Omega)}\sinh\left[\Gamma(\vec{q},\Omega)\right], \tag{7b}$$

$$\varphi(\vec{q},\Omega) = \frac{k_s(\vec{q},\Omega) - k_s(-\vec{q},-\Omega)}{2}l_c, \tag{7c}$$

$$\Gamma(\vec{q},\Omega) = \sqrt{g^2 - \frac{\Delta^2_{\mathrm{pw}}(\vec{q},\Omega)l_c^2}{4}}, \tag{7d}$$

$$\Delta_{\mathrm{pw}}(\vec{q},\Omega) = k_{sz}(\vec{q},\Omega) + k_{sz}(-\vec{q},-\Omega) - k_p, \tag{7e}$$

where $k_p = k_{pz}(0,0)$.

We note that the functions $U(\vec{q},\Omega)$ and $V(\vec{q},\Omega)$ satisfy the conditions:

$$\begin{aligned} &|U(\vec{q},\Omega)|^2 - |V(\vec{q},\Omega)|^2 = 1, \\ &U(\vec{q},\Omega)V(-\vec{q},-\Omega) = U(-\vec{q},-\Omega)V(\vec{q},\Omega), \end{aligned} \tag{8}$$

necessary to preserve the commutation relations from the input to the output face of the crystal.

Once we have found the solution to the propagation equation, i.e. we have an explicit expression for the field at the output face of the crystal, we can evaluate the quantity of primary interest when dealing with the PDC entangled state, the so called *biphoton amplitude*:

$$\psi(\vec{x},t,\vec{x}',t') = \langle \hat{A}_s(\vec{x},t)\hat{A}_s(\vec{x}',t')\rangle. \tag{9}$$

The biphoton amplitude, i.e. the biphoton cross-correlation, is the quantity at the heart of the photon-pair PDC entanglement: the "anomalous" propagator into Eq. (9) is, indeed, characteristic of processes where particles are created in pairs.

Thanks to Eq. (6) we can easily evaluate the plane wave pump (PWP) result for the biphoton amplitude:

$$\begin{aligned} \psi(\vec{x},t,\vec{x}',t') &= \langle \hat{A}_s(\vec{x},t)\hat{A}_s(\vec{x}',t')\rangle \\ &= \int \frac{d^2\vec{q}d\Omega}{2\pi^{3/2}}\int \frac{d^2\vec{q}'d\Omega'}{2\pi^{3/2}}\langle \hat{A}_s(\vec{q},\Omega)\hat{A}_s(\vec{q}',\Omega')\rangle \mathrm{e}^{i(\vec{q}\cdot\vec{x}-\Omega t)}\mathrm{e}^{i(\vec{q}'\cdot\vec{x}'-\Omega' t')} \\ &= \int \frac{d^2\vec{q}d\Omega}{(2\pi)^3}\mathrm{e}^{i\vec{q}\cdot(\vec{x}-\vec{x}')-i\Omega(t-t')}U(\vec{q},\Omega)V(-\vec{q},-\Omega), \end{aligned} \tag{10}$$

where we exploit the well known commutation relation

$$[\hat{A}_s(\vec{q},\Omega,0),\hat{A}_s^\dagger(\vec{q}',\Omega',0)] = \delta(\vec{q}-\vec{q}')\delta(\Omega-\Omega'), \tag{11}$$

and the identities $\langle \hat{A}_s\hat{A}_s\rangle = \langle \hat{A}_s^\dagger\hat{A}_s\rangle = \langle \hat{A}_s^\dagger\hat{A}_s^\dagger\rangle = 0$, deriving from the fact that the signal field at input face of the crystal is in the vacuum state. We notice that the biphoton amplitude is proportional to g. We note that the biphoton

amplitude depends only on the relative coordinates $\vec{\xi} = \vec{x} - \vec{x}'$ and $\tau = t - t'$, as it is natural to expect for an homogeneous and stationary pump.

We need therefore to calculate the Fourier transform of the function $F(\vec{q}, \Omega) = U(\vec{q}, \Omega)V(-\vec{q}, -\Omega)$:

$$\psi(\vec{\xi}, \tau) = \int \frac{d^2\vec{q}d\Omega}{(2\pi)^3} \mathrm{e}^{i\vec{q}\cdot\vec{\xi} - i\Omega\tau} F(\vec{q}, \Omega)\,, \tag{12a}$$

$$F(\vec{q}, \Omega) = \frac{g\mathrm{e}^{ik_p l_c}}{\Gamma(\vec{q}, \Omega)} \sinh\left[\Gamma(\vec{q}, \Omega)\right] \left\{ \cosh\left[\Gamma(\vec{q}, \Omega)\right] + i\frac{\Delta_{\mathrm{pw}}(\vec{q}, \Omega) l_c}{2\Gamma(\vec{q}, \Omega)} \sinh\left[\Gamma(\vec{q}, \Omega)\right] \right\} \tag{12b}$$

where in Eq. (12b) we used the identity $\varphi(-\vec{q}, -\Omega) = -\varphi(\vec{q}, \Omega)$.

We note that $F(\vec{q}, \Omega)$ depends on variables $(\vec{q}, \Omega)$ only through the function $\Delta_{\mathrm{pw}}(\vec{q}, \Omega)$, that for the case of e-oo type I parametric down-conversion considered in this section, has radial symmetry with respect to $\vec{q}$: $\Delta_{\mathrm{pw}}(\vec{q}, \Omega) = \Delta_{\mathrm{pw}}(q, \Omega)$, where $q = |\vec{q}|$. We can therefore evaluate Eq. (12) by mean of a Fourier-Hankel transform:

$$\psi(\xi, \tau) = \int_{-\infty}^{\infty} \frac{d\Omega}{2\pi} \mathrm{e}^{-i\Omega\tau} \int_0^{\infty} \frac{dq}{2\pi} q F(q, \Omega) J_0(q \cdot \xi)\,, \tag{13}$$

where

$$J_0(x) = \frac{1}{2\pi} \int_0^{2\pi} \mathrm{e}^{i\sin(\theta)x} d\theta \tag{14}$$

is the fisrt order Bessel function of the first kind. It is evident from Eq. (13) that the biphoton amplitude depends only on the radial coordinate ξ, i.e. on the relative distance of the down-converted photons.

We numerically evaluate Eq. (13) for a type I 4mm long BBO crystal, pumped at $\lambda_p = 352$nm, cut at 33.426° for collinear phase matching at degeneracy, with $g = 10^{-3}$. In order to select an appropriate range of wavelengths, consistent for example with the finite bandwidth of detection, we introduce a symmetrical frequency filter centered at degeneracy with a super-gaussian profile with a full width at half maximum (FWHM) of 1370 THz, corresponding to a wavelength band from 550 nm to 950 nm.

The results are shown in Fig.1: in panel (a) we report the two dimensional cut of the biphoton amplitude at $\xi_y = 0$, clearly displaying its X-structure, non separable in space and time. The whole 3-dimensional plot has a rotational symmetry in space, as shown in Fig.1(b), where we plot the isosurface obtained for the particular value $|\psi(\vec{\xi}, \tau)|/|\psi(0, 0, 0)| = 0.15$. A clear X-shaped structure emerges: this non-trivial shape of the spatio-temporal two-photon correlation, that we shall call *X-entanglement* can be considered the counterpart, at the quantum level, of the nonlinear X-waves [20].

A remarkable characteristic of the X-entanglement is the unusually small width of the spatio-temporal correlation peak, which corresponds to a strong relative localization of twin photons both in time and space. The two lower frames of Fig.1 plot cuts of the two-photon coincidence rate $|\psi|^2$ along the temporal

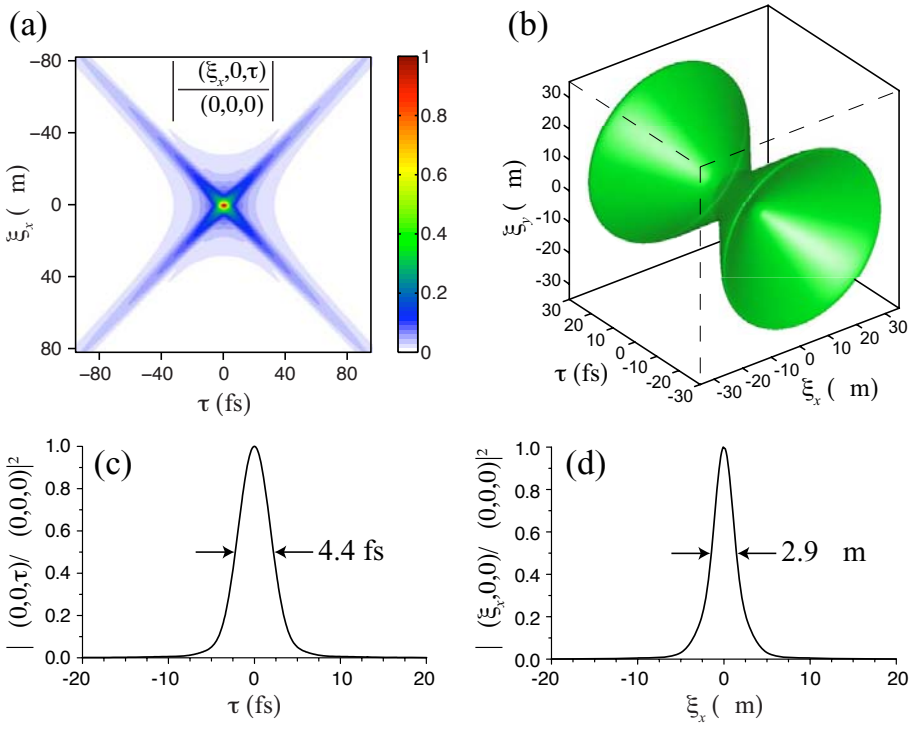

Fig. 1. (color online) (a) Two dimensional plot of the section of the biphoton amplitude for $\xi_y = 0$, normalized to its peak value $\psi(0,0,0)$, clearly showing its X-shaped geometry. (b) Isosurface representing the full 3-dimensional structure of the biphoton amplitude (in modulus), for the particular value $|\psi(\vec{\xi},\tau)|/|\psi(0,0,0)| = 0.15$. In the lower panels we report the one dimensional section of the coincidence rate $|\psi|^2$ along the temporal (c) and spatial (d) coordinate axis. The widths of the peaks shows the relative temporal and spatial localization of biphotons. We consider a 4mm-long type I BBO crystal cut at 33.436° for collinear phase matching at degeneracy, $g = 10^{-3}$, $\lambda_p = 352$nm.

and spatial axis, respectively. The relative spatial localization is remarkable but not impressive, as displayed in Fig.1(d) by the $|\psi(\xi_x,0,0)|^2$ spatial profile, obtained for $\tau = 0$, which has a FWHM of $\sim 2.9\,\mu$m. More impressive, and in a sense, unexpected, is the relative localization in time of twin photons, which can be appreciated from the temporal profile $|\psi(0,0,\tau)|^2$ in Fig.1(c), which is as narrow as 4.4 fs. Such an ultra-short two-photon localization emerges spontaneously from a monochromatic pump, as a consequence of the ultra-broad bandwidth of PDC phase-matching, which in principle extends over the optical frequency $\omega_p \sim 5 \cdot 10^{15}$ Hz.

It is interesting to compare our results with the typical $\sim$ 100 fs temporal localization of the coincidence rate measured in the far-field zone, by collecting twin photons that propagate at symmetric directions $\vec{q}$ and $-\vec{q}$, within a

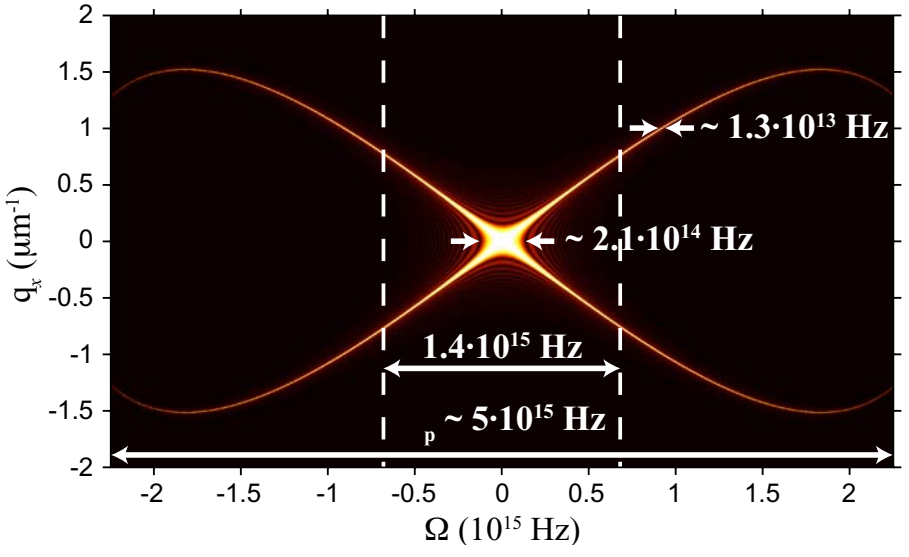

Fig. 2. (Color online) Plot of $|F|$, showing the phase matching curve in the (q_x, Ω) plane. The dashed lines show the bandwidth selected by the filter and the arrows indicate the different bandwidths involved (same parameters as in Fig.1).

small angular bandwidth. In that case, the measured quantity is proportional to $|F(\vec{q},\tau)|^2 = |\int \frac{d\Omega}{2\pi} e^{-i\Omega\tau} F(\vec{q},\Omega)|^2$. Its temporal width is determined by the inverse of the bandwidth of $F(\vec{q},\Omega)$ at fixed q, i.e. the narrow ($10^{13} - 10^{14}$Hz) thickness of the curve in Fig.2. This bandwidth can be roughly evaluated as Ω_0 for $q/q_0 << 1$, and as $\Omega_0 q_0/q$ for $q/q_0 > 1$, where $\Omega_0 = \sqrt{1/k_s'' l_c}$, $q_0 = \sqrt{k_s/l_c}$, and we used the short-hand notation $k_s = k_s(0,0)$, $k_s'' = d^2k_s/d\Omega^2|_{0,0}$. Clearly, since Ω_0 scales as $l_c^{-1/2}$, the shorter the crystal, the stronger the temporal localization in the far-field; however, a far-field localization in the femtosecond range would require a crystal as short as $\sim 50\,\mu$m, with a strongly reduced down-conversion efficiency. Conversely, in our case, the detection of coincidences in the near-field gives in principle access to the full ($\sim 10^{15}$Hz) bandwidth of phase matching even for a long crystal.

It is however important to stress that such an extreme temporal localization of twin photons relies on the ability to resolve their relative position in the near-field plane. Indeed, a measurement collecting all the photons over the beam cross-section, without discriminating their positions, is characterized by the integrated coincidence rate $\int d^2\vec{\xi}\,|\psi(\vec{\xi},\tau)|^2$, which for the case considered here, has a width of ∼100fs.

In Fig.3 we compare the standard deviation of the coincidence rate when resolving the near-field position of twin photons $|\psi(\vec{\xi}=0,\tau)|^2$ (red solid line), with the integrated coincidence rate $\int d^2\vec{\xi}\,|\psi(\vec{\xi},\tau)|^2$ (black dashed line), for different crystal lengths. For a thin crystal with $l_c = 0.1$mm (Fig.3(a)), the standard deviations of the two distribution are almost the same, while it is clearly evident the

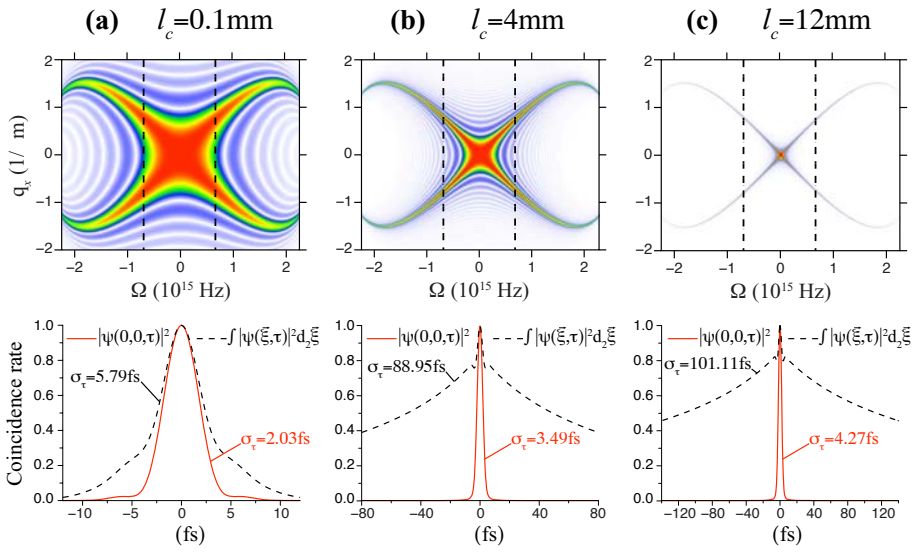

Fig. 3. (color online) Section of $|F(\vec{q},\Omega)|$ in the (q_x,Ω) plane (upper panels), for different crystal lengths: (a) $l_c = 0.1$mm, (b) $l_c = 4$mm and (c) $l_c = 12$mm. Lower panels: comparison between the coincidence rate when twin photons are collected at the same near-field position ($|\psi(\xi=0,\tau)|^2$, solid line) and the coincidence rate measured without resolving photon positions ($\int d^2\xi\,|\psi(\xi,\tau)|^2$, dashed line), for the different crystal lengths considered.

difference as the crystal length increases: even for a long crystal, that means an high efficiency for the down conversion process, the temporal localization of twin photons is on the order of few fs if we resolve their near-field position, while it is two order of magnitude greater if we consider the integrated coincidence rate (Fig.3(c)).

It may appear surprising that when the photons are collected without discriminating their near-field position, their temporal localization is determined by the inverse of the bandwidth of $F(q,\Omega)$ at fixed q rather than by the inverse of the full phase-matching bandwidth, because in this measurement all the photons at the different frequencies within the phase-matching are collected. However, the identity $\int d^2\vec{\xi}\,|\psi(\vec{\xi},\tau)|^2 = \int d^2\vec{q}|F(\vec{q},\tau)|^2$ shows that in this case the coincidence rate takes the form of an *incoherent superposition* of the probabilities of detecting a pair of photons at a given q and has therefore the same ~ 100fs temporal localization as the far-field coincidence rate at fixed q. Conversely, by resolving the near-field positions of twin photons, the measured quantity is $|\psi(0,0,\tau)|^2 = |\int \frac{d^2\vec{q}}{(2\pi)^2} F(\vec{q},\tau)|^2$, which corresponds to a *coherent superposition* of the probability amplitudes at a given q (i.e. at a given frequency due to the the angle-frequency relation imposed by phase matching), and therefore allows a stronger temporal localization.

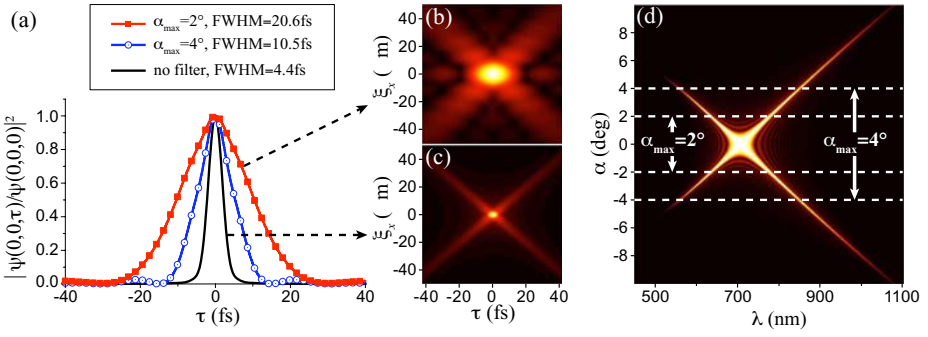

Fig. 4. (Color online) Effect of spatial filtering on the X-entanglement: (a) Temporal correlation peak $|\psi(0,0,\tau)|^2$ in the presence of a spatial filter, that cuts the angular spectrum at an angle $\alpha_{\max}$. The two insets show the full X-correlation for $\alpha_{\max} = 2^0$ (b), and in the absence of the spatial filter (c). As the angular cut-off α_{max} is reduced, the temporal peak broadens, as a consequence of the non-factorability in space-time, as illustrated by panel (d) that shows how an angular cut-off also cuts the temporal spectrum, due to the angular dispersion relation of PDC.

The non-factorability in space and time of the X-entanglement thus opens the relevant possibility of tailoring the temporal bandwidth of the biphotons by acting on their spatial degrees of freedom. As a specific example, let us consider the effects of spatial filtering on the temporal correlation. Let us assume that a $4f$ lens system is employed to image the near-field of the PDC fluorescence, and that a circular aperture of radius r_a is located in the far-field $2f$ plane, acting as a filter that cuts all the angular spectrum at $\alpha > \alpha_{\max} = \arcsin(r_a/f)$. Fig. 4 shows the effect of such a spatial filter on the temporal correlation peak. While in the absence of any spatial filter the correlation shows a strong temporal localization, as the angular bandwidth is reduced by spatial filtering, the two-photon correlation broadens in time.

This is a clear effect of the non-factorability of the correlation in space and time, as can be understood by inspection of Fig. 4(d), that shows how a spatial filter that cuts the angular spectrum at an angle α_{max} has also the effect of cutting the temporal bandwith. In turns, this implies a broadening of the temporal correlation peak, so that the relative temporal localization of twin photons deteriorates.

3 Type II Parametric Down Conversion

In this section we shall investigate how the spatio-temporal structure of the biphoton amplitude behaves in a type II phase-matching configuration, outlining the similarity and the differences with respect to the type I phase-matching case. We will show in particular that the nonfactorable character with respect to the space-time coordinates persists and the strong temporal localization is

similar to that found in type I phase-matching. However, at low gains the biphotonic structure is highly asymmetric with respect to the temporal dimension, because of the group velocity mismatch (GVM) between the signal and the idler fields. It is known, indeed, that the GVM affecting type II PDC produces this temporal asymmetry (see e.g. [35]), because of the temporal lag of the "slow" photons with respect to the "fast" photons. This asymmetry is not present in the type I configuration, as the GVM is vanishingly small in the neighborhood of the degenerate frequency. By considering the full spatio-temporal structure of entanglement, we shall see that the asymmetry characterizing type II PDC makes the biphoton correlation function looks like a truncated X which is somewhat similar to a Y (the truncation regarding the temporal region corresponding to anticipitated arrival times of the "slow" photons). It turns out, however, that this asymmetry tends to disappear as the parametric gain is raised: a transition from an Y-shaped to an X-shaped structure is indeed observed, recovering thereby the symmetrical structure encountered in type I phase-matching.

Following also for the type II PDC the model described by Gatti *et al.*[25, 32, 31], we can find an equation similar to Eq. (4) for both the signal and idler field:

$$\frac{\partial \hat{a}_j(\vec{q},\Omega,z)}{\partial z} = \frac{g}{l_c}\int\frac{d^2\vec{q}'}{2\pi}\int\frac{d\Omega'}{\sqrt{2\pi}}\bar{\alpha}_p(\vec{q}+\vec{q}',\Omega+\Omega')\hat{a}_l^\dagger(\vec{q}',\Omega',z)\mathrm{e}^{-i\Delta_{jl}(\vec{q},\Omega;\vec{q}',\Omega')z}\,, \qquad j\neq l=s,i\,, \tag{15}$$

where the subscripts s and i represent the signal and idler fields, respectively, and

$$\Delta_{jl}(\vec{q},\Omega;\vec{q}',\Omega') = k_{jz}(\vec{q},\Omega)+k_{lz}(\vec{q}',\Omega')-k_{pz}(\vec{q}+\vec{q}',\Omega+\Omega')\,. \tag{16}$$

For a monochromatic and plane wave pump, as shown in the previous section, the propagation equation (15) has an analytic solution, that takes the form:

$$\begin{aligned}\hat{A}_s(\vec{q},\Omega) &= U_s(\vec{q},\Omega)\hat{A}_s(\vec{q},\Omega,0)+V_i(\vec{q},\Omega)\hat{A}_i^\dagger(-\vec{q},-\Omega,0)\,,\\ \hat{A}_i(\vec{q},\Omega) &= U_i(\vec{q},\Omega)\hat{A}_i(\vec{q},\Omega,0)+V_s(\vec{q},\Omega)\hat{A}_s^\dagger(-\vec{q},-\Omega,0)\,,\end{aligned} \tag{17}$$

where

$$\begin{aligned}U_s(\vec{q},\Omega) &= U(\vec{q},\Omega)\mathrm{e}^{i\varphi(\vec{q},\Omega)}\\ V_s(\vec{q},\Omega) &= V(\vec{q},\Omega)\mathrm{e}^{i\varphi(\vec{q},\Omega)}\\ U_i(\vec{q},\Omega) &= U(-\vec{q},-\Omega)\mathrm{e}^{-i\varphi(-\vec{q},-\Omega)}\\ V_i(\vec{q},\Omega) &= V(-\vec{q},-\Omega)\mathrm{e}^{-i\varphi(-\vec{q},-\Omega)}\end{aligned} \tag{18}$$

with the same definitions as in Eq. (7), with

$$\Delta_{\mathrm{pw}}(\vec{q},\Omega) = k_{sz}(\vec{q},\Omega)+k_{iz}(-\vec{q},-\Omega)-k_p\,, \tag{19}$$

and

$$\varphi(\vec{q},\Omega) = \left[k_{sz}(\vec{q},\Omega) - k_{iz}(-\vec{q},-\Omega)\right]\frac{l_c}{2}\,. \tag{20}$$

It can be shown [36] that in this case the biphoton amplitude takes the form:

$$\psi(\vec{\xi},\tau) = \int \frac{d^2\vec{q}}{(2\pi)^2}\int \frac{d\Omega}{2\pi}\mathrm{e}^{i\vec{q}\cdot\vec{\xi}-i\Omega\tau}U_s(\vec{q},\Omega)V_i(-\vec{q},-\Omega)\,. \tag{21}$$

As in the previous section we need to numerically evaluate Eq. (21), but in this case it is not straightforward the reduction to a 2-dimensional integral, since we can not exploit the radial symmetry, because of the different polarization of signal and idler fields. Nevertheless, considering the paraxial approximation and an appropriate change of variables, we have:

$$\psi(\vec{\xi},\tau) = \frac{1}{\beta_{xx}\beta_{yy}}\int \frac{d\Omega}{2\pi}\mathrm{e}^{-i\Omega t}\mathrm{e}^{iq_c(\Omega)\xi}\int_0^\infty \frac{dq}{2\pi}qJ_0(q\cdot\xi)F_{si}(q,\Omega)\,, \tag{22}$$

where

$$F_{si}(\vec{q},\Omega) \equiv U_s(\vec{q},\Omega)V_i(-\vec{q},-\Omega)\,, \tag{23}$$

and an explicit expression for the coefficients β_{xx}, β_{yy} and for the function $q_C(\Omega)$ can be found in [36].

For the numerical evaluation of ψ given by Eq. (22), we first evaluated the Fourier-Hankel transform by using the quadrature method illustrated in [37] which offers an excellent precision level. The Fourier transform with respect to the temporal frequency was then evaluated using the FFT based on Bluestein algorithm which allows to select an appropriate time window within the Nyquist interval without resorting to zero-padding. Especially at low gain, the slow decaying and strongly oscillating behaviour of F_{si} requires a large number of quadrature points, so that the direct evaluation of the (2+1)D transform given in Eq. (21) would have been much more demanding, if not prohibitive, from the point of view of both computation times and memory use.

In order to evaluate numerically the biphoton amplitude $\psi(\xi,\tau)$ we focus our attention on the specific case of a 4mm long BBO crystal cut for type II phase-matching with an injected plane-wave pump field at $\lambda_p = 352$nm. We first consider a regime of low parametric gain, by taking $g = 0.001$. Assuming the pump axis z is taken at an angle $\theta_p = 49.05^\circ$ with the crystal axis, collinear phase-matching occurs at the degenerate frequency $\lambda_s = \lambda_i = 704$nm.

Figure 5(a) maps the large scale phase-matching curves $\Delta_{\mathrm{pw}}(q_x, q_y = 0, \Omega) = 0$ of both the signal and idler waves in the plane corresponding to the walk-off direction. For this particular phase-matching configuration the two curves are almost tangent close to degeneracy, in the region where nearly collinear emission takes place (i.e. for $\lambda \sim 2\lambda_p$ and $\vec{q} \sim 0$). In Fig.5(b) the modulus of the complex function we have to Fourier transform, namely $F_{si}(\vec{q},\Omega)$, is mapped with a grayscale image in the in the (q_x,Ω) plane. Its maximum values (in white) clearly reproduces the signal phase-matching curve shown in the left panel. We included also in this case the multiplication by the frequency filter described into the previous section.

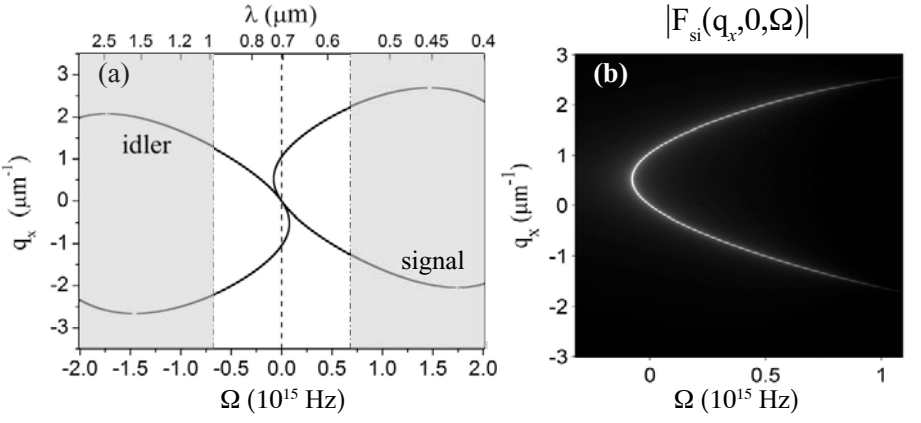

Fig. 5. (a) Large scale plot of the phase-matching curves $\Delta_{\rm pw}(q_x, q_y = 0, \Omega) = 0$ of the signal and idler waves in the walk-off plane. The unshaded region centered at degeneracy corresponds to the chosen frequency range selected by the super-Gaussian filter. (b) Grayscale plot of $|F_{si}(q_x, q_y = 0, \Omega)|$ in the same plane, modulated by the super-Gaussian frequency filter.

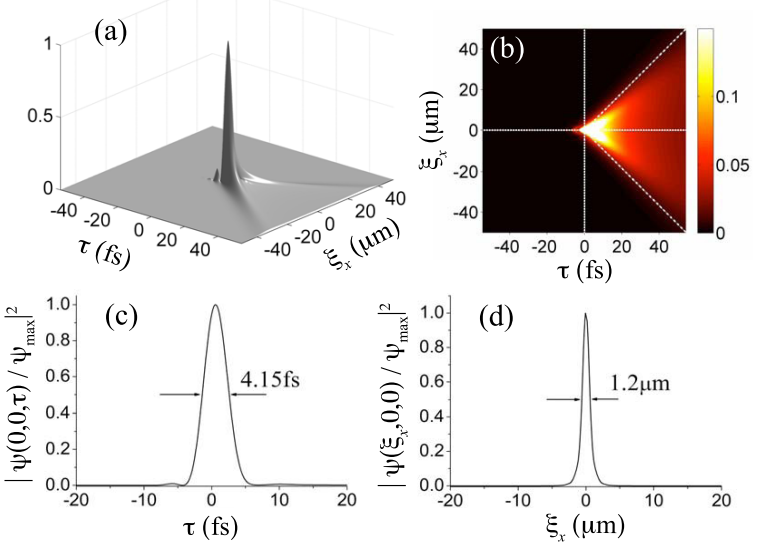

Fig. 6. (Color online) (a) and (b) Structure of the biphoton amplitude on a fs/μm scale. The plots in panels (c) and (d) show the profile of the coincidence rate $|\psi(\xi, \tau)|^2$ along the temporal and the transverse ξ_x-axis, respectively [the cuts are indicated by the two dashed lines in frame (b)]. The FWHM of the correlation peaks (indicated in the figures) gives a measure the relative localization of biphotons in space and in time.

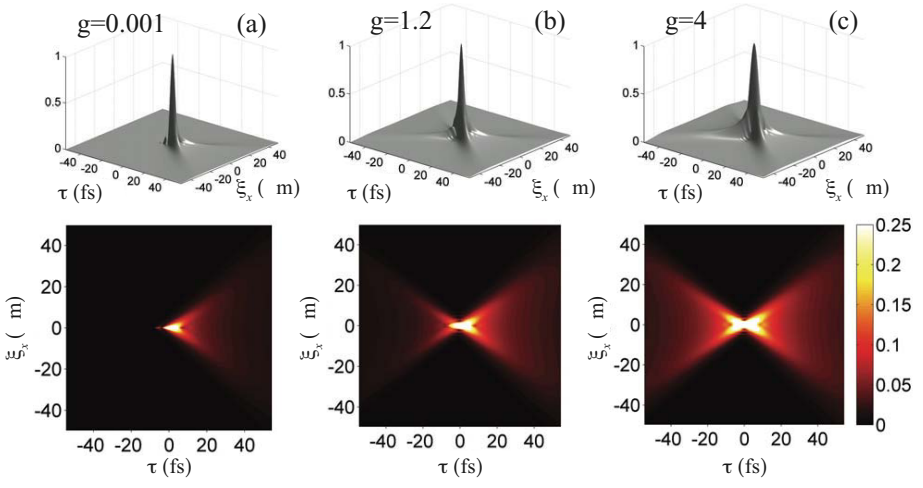

Fig. 7. (Color online) Behavior of the biphoton correlation in the (ξ_x, τ) plane for increasing value of the parametric gain. The color map of the 2D plot below is truncated to 1/4 of the peak value of $|\psi|$ to enhance the contrast of the tails.

Figure 6 displays the modulus of biphoton amplitude in the (ξ_x, τ) plane on a femtosecond/micrometer scale in order to put in evidence the strong relative localization of the twin photons in space and time. We have a kind of Y-shaped structure (the Y being clock-wise rotated to 90^o in the plot of Fig.6(b)) that clearly does not factorize with respect to the space-time coordinates and that extends mainly in the positive τ half-plane. Regarding this last feature, the structure is qualitatively different from that found in the previous section for type I phase-matching configuration, which is perfectly symmetric both with respect to the temporal and spatial relative position and appears as X-shaped in the (ξ_x, τ) plane. The tails direction in the (ξ_x, τ) plane is related to the asymptotic behaviour of the phase-mismatch function $\Delta_{\rm pw}(\vec{q}, \Omega)$ for large Ω. If we consider the paraxial and quadratic dispersion approximation for $\Delta_{\rm pw}(\vec{q}, \Omega)$ (for details see Brambilla *et al.*[36]), we obtain the relation $\tau = \pm\sqrt{\frac{2k_s k_i (k_s'' + k_i'')}{k_s + k_i}}\xi$ corresponding to the two diagonals indicated with the dashed lines in Fig.6(b).

As can be seen from temporal profile shown in Fig.6(c) the biphoton correlation is trongly localized with a FWHM as narrow as 4.15fs, which is quite close to that found for the type I configuration.

To go deep into the understanding of the biphoton amplitude spatiotemporal structure, we evaluated numerically the biphoton amplitude by increasing the parametric gain. As can be seen from Fig.7, when g is raised, diagonal tails that mirror those in the $\tau > 0$ half-plane develops in the $\tau < 0$ half-plane. Thus, the strong asymmetry along the temporal axis that characterizes the low gain regime (see Fig.7(a)) progressively disappears and a transition from an Y-shaped to an X-shaped structure is observed. We can explain qualitatively

this behaviour noticing that the vacuum fluctuations that trigger spontaneous PDC are exponentially amplified in a regime of high parametric gain, as the produced photon pairs stimulate the generation of many other photon pairs in a kind of cascading process. The "slow" signal photons can thus be generated in processes stimulated by the "faster" idler photons and vice versa, so that the arrival time distributions of the signal and the idler photons tend to overlap when this cascading effect becomes dominant in the production of photon pairs. As a result, the strong assymetry of the correlation function along the temporal axis, that reveals the temporal delay of the "slow" signal photons with respect to the idler photons in the low gain regime, disappears pregressively when the parametric gain is raised.

4 Conclusions

In conclusion, this work demonstrates that the X-geometry is intrinsic to PDC at the microscopic quantum level of photon-pair entanglement. As for the macroscopic X-waves and the classical phase coherence of PDC [22, 23], the non-factorability is imposed by the phase-matching mechanism governing the wave-mixing processes. Following this analogy, we coined the name of X-entanglement. The key element of novelty that emerges in the microscopic context is the extreme relative localization of twin photons, with correlation times and correlation lengths in the femtosecond and micrometer range, respectively. The strong temporal localization is determined by the full extent of the PDC bandwidth, rather than by the bandwidth $\sim \Omega_0$ characterizing the PDC far-field. For this reason, a near-field measurement scheme able to resolve spatially the coincidences would provide a powerful tool for high-precision measurements, capable of improving substantially the resolution power in the temporal domain with respect to standard schemes.

Moreover this extreme temporal localization emerges spontaneously from a monochromatic pump, and persists even for long crystals, where on the contrary usual measurement schemes give correlation times on the order of hundreds of fs, for both type I and type II parametric down conversion. This is very striking, as the GVM characterizing the type II PDC leads to signal-idler temporal walk-off typically in the picosecond range. We verified that in the coincidence regime the GVM generates an aymmetry in the biphoton amplitude along the temporal dimension which progressively disappears as the parametric gain is increased, and a transition from a Y to an X-shaped structure is observed. On the other hand the temporal and the spatial localizations are almost preserved as the parametric gain increases.

Acknowledgments

Work supported by the FET programme of the EC, under the GA HIDEAS FP7-ICT-221906.

References

[1] Duan, L.-M., Lukin, M.D., Cirac, J.I., Zoller, P.: Long-distance quantum communication with atomic ensembles and linear optics. Nature 414, 413 (2001)

[2] Lloyd, S., Shahriar, M.S., Shapiro, J.H., Hemmer, P.R.: Long distance, unconditional teleportation of atomic states via complete bell state measurements. Phys. Rev. Lett. 87(16), 167903 (2001)

[3] Du, S., Kolchin, P., Belthangady, C., Yin, G.Y., Harris, S.E.: Subnatural linewidth biphotons with controllable temporal length. Phys. Rev. Lett. 100(18), 183603 (2008)

[4] Neergaard-Nielsen, J.S., Nielsen, B.M., Takahashi, H., Vistnes, A.I., Polzik, E.S.: High purity bright single photon source. Opt. Express 15(13), 7940–7949 (2007)

[5] Abouraddy, A.F., Nasr, M.B., Saleh, B.E.A., Sergienko, A.V., Teich, M.C.: Quantum-optical coherence tomography with dispersion cancellation. Phys. Rev. A 65(5), 053817 (2002)

[6] Nasr, M.B., Saleh, B., Sergienko, A., Teich, M.: Dispersion-cancelled and dispersion-sensitive quantum optical coherence tomography. Opt. Express 12(7), 1353–1362 (2004)

[7] Giovannetti, V., Lloyd, S., Maccone, L.: Quantum-enhanced positioning and clock synchronization. Nature 412, 417–419 (2001)

[8] Giovannetti, V., Lloyd, S., Maccone, L., Wong, F.N.C.: Clock synchronization with dispersion cancellation. Phys. Rev. Lett. 87(11), 117902 (2001)

[9] Dauler, E., Jaeger, G., Muller, A., Migdall, A., Sergienko, A.: Tests of a two-photon technique for measuring polarization mode dispersion with subfemtosecond precision. J. Res. Natl. Inst. Stand. Technol. 104(1), 1 (1999)

[10] Carrasco, S., Torres, J.P., Torner, L., Sergienko, A., Saleh, B.E.A., Teich, M.C.: Enhancing the axial resolution of quantum optical coherence tomographyby chirped quasi-phase matching. Opt. Lett. 29(20), 2429–2431 (2004)

[11] Harris, S.E.: Chirp and compress: Toward single-cycle biphotons. Phys. Rev. Lett. 98(6), 063602 (2007)

[12] Nasr, M.B., Carrasco, S., Saleh, B.E.A., Sergienko, A.V., Teich, M.C., Torres, J.P., Torner, L., Hum, D.S., Fejer, M.M.: Ultrabroadband biphotons generated via chirped quasi-phase-matched optical parametric down-conversion. Phys. Rev. Lett. 100(18), 183601 (2008)

[13] Nasr, M.B., Minaeva, O., Goltsman, G.N., Sergienko, A.V., Saleh, B.E., Teich, M.C.: Submicron axial resolution in an ultrabroadband two-photon interferometer using superconducting single-photon detectors. Opt. Express 16(19), 15104–15108 (2008)

[14] Nasr, M.B., Giuseppe, G.D., Saleh, B.E., Sergienko, A.V., Teich, M.C.: Generation of high-flux ultra-broadband light by bandwidth amplification in spontaneous parametric down conversion. Opt. Comm. 246(4-6), 521–528 (2005)

[15] O'Donnell, K.A., U'Ren, A.B.: Observation of ultrabroadband, beamlike parametric downconversion. Opt. Lett. 32(7), 817–819 (2007)

[16] Carrasco, S., Torres, J.P., Torner, L., Sergienko, A., Saleh, B.E.A., Teich, M.C.: Spatial-to-spectral mapping in spontaneous parametric down-conversion. Phys. Rev. A 70, 043817 (2004)

[17] Carrasco, S., Sergienko, A.V., Saleh, B.E.A., Teich, M.C., Torres, J.P., Torner, L.: Spectral engineering of entangled two-photon states. Phys. Rev. A 73(6), 063802 (2006)

[18] Carrasco, S., Nasr, M.B., Sergienko, A.V., Saleh, B.E., Teich, M.C., Torres, J.P., Torner, L.: Broadband light generation by noncollinear parametric downconversion. Opt. Lett. 31(2), 253–255 (2006)

[19] Hendrych, M., Shi, X., Valencia, A., Torres, J.P.: Broadening the bandwidth of entangled photons: A step towards the generation of extremely short biphotons. Phys. Rev. A 79(2), 023817 (2009)
[20] Conti, C., Di Trapani, P., Trillo, S.: X-waves in self-focusing of ultra-short pulses. In: Boyd, R.W., Lukishova, S.G., Shen, Y.R. (eds.) Self-focusing: Past and Present. Topics in Applied physics, ch. 18, vol. 114, pp. 439–456. Springer, Heidelberg (2009)
[21] Gaižauskas, E., Dubietis, A., Kudriašov, V., Sirutkaitis, V., Couairon, A., Faccio, D., Di Trapani, P.: On the role of conical waves in self-focusing and filamentation of femtosecond pulses with nonlinear losses. In: Boyd, R.W., Lukishova, S.G., Shen, Y.R. (eds.) Self-focusing: Past and Present, ch. 19, vol. 114, pp. 457–479. Springer, Heidelberg (2009)
[22] Jedrkiewicz, O., Picozzi, A., Clerici, M., Faccio, D., Trapani, P.D.: Emergence of x-shaped spatiotemporal coherence in optical waves. Phys. Rev. Lett. 97(24), 243903 (2006)
[23] Jedrkiewicz, O., Clerici, M., Picozzi, A., Faccio, D., Trapani, P.D.: X-shaped space-time coherence in optical parametric generation. Phys. Rev. A 76(3), 033823 (2007)
[24] Atatüre, M., Di Giuseppe, G., Shaw, M.D., Sergienko, A.V., Saleh, B.E.A., Teich, M.C.: Multiparameter entanglement in femtosecond parametric down-conversion. Phys. Rev. A 65(2), 023808 (2002)
[25] Gatti, A., Zambrini, R., Miguel, M.S., Lugiato, L.A.: Multiphoton multimode polarization entanglement in parametric down-conversion. Phys. Rev. A 68, 053807 (2003)
[26] Hong, C.K., Ou, Z.Y., Mandel, L.: Measurement of subpicosecond time intervals between two photons by interference. Phys. Rev. Lett. 59(18), 2044 (1987)
[27] Law, C.K., Walmsley, I.A., Eberly, J.H.: Continuous frequency entanglement: Effective finite hilbert space and entropy control. Phys. Rev. Lett. 84(23), 5304 (2000)
[28] Grice, W.P., U'Ren, A.B., Walmsley, I.A.: Eliminating frequency and space-time correlations in multiphoton states. Phys. Rev. A 64(6), 063815 (2001)
[29] Rubin, M.H.: Transverse correlation in optical spontaneous parametric down-conversion. Phys. Rev. A 54(6), 5349 (1996)
[30] Law, C.K., Eberly, J.H.: Analysis and interpretation of high transverse entanglement in optical parametric down conversion. Phys. Rev. Lett. 92(12), 127903 (2004)
[31] Gatti, A., Brambilla, E., Lugiato, L.A.: Quantum Imaging. In: Wolf, E. (ed.) Progress in Optics, vol. 51, ch. 5, pp. 251–348. Elsevier B.V., Amsterdam (2008)
[32] Brambilla, E., Gatti, A., Bache, M., Lugiato, L.: Simultaneous near-field and far field spatial quantum correlations in the high-gain regime of parametric down-conversion. Phys. Rev. A 69, 023802 (2004)
[33] Gatti, A., Brambilla, E., Caspani, L., Jedrkiewicz, O., Lugiato, L.A.: X entanglement: The nonfactorable spatiotemporal structure of biphoton correlation. Physical Review Letters 102(22), 223601 (2009)
[34] Caspani, L., Brambilla, E., Lugiato, L.A., Gatti, A.: Tailoring the spatio-temporal structure of biphoton entanglement in type I parametric down conversion (submitted, 2009)
[35] Rubin, M.H., Klyshko, D.N., Shih, Y.H., Sergienko, A.V.: Theory of two-photon entanglement in type-II optical parametric down-conversion. Phys. Rev. A 50(6), 5122 (1994)
[36] Brambilla, E., Caspani, L., Lugiato, L.A., Gatti, A.: Spatio-temporal structure of biphoton entanglement in type II PDC (in preparation, 2009)
[37] Yu, L., Huang, M., Chen, M., Chen, W., Huang, W., Zhu, Z.: Quasi-discrete hankel transform. Opt. Lett. 23(6), 409 (1998)